Plasmonic bandpass filters with cascaded rectangular ring resonators

Chyong-Hua Chen

Department of Photonics and Institute of Electro-Optical Engineering, National Chiao Tung University, 1001 TaHsueh Road, Hsinchu 30010, Taiwan (chyong@mail.nctu.edu.tw)

Received February 26, 2014; revised April 10, 2014; accepted April 15, 2014; posted April 16, 2014 (Doc. ID 207147); published May 26, 2014

We theoretically present the analysis and design of a nanoplasmonic bandpass filter with flat-top spectral characteristics by cascading a series of directly connected rectangular ring resonators based on metal–insulator–metal waveguides. Analyzed by the equivalent lumped circuit model of the transmission line to plasmonic waveguides, the transmission properties of a symmetric rectangular ring resonator with the directly connected input and output waveguides are approximately the same as that of a Fabry–Perot resonator. Then the thin-film design methodology is applied to realize a plasmonic bandpass filter with the squared passband. An example of cascaded two-rectangular ring resonator structure is numerically demonstrated by using the transmission line model and 2D finite difference time domain method. © 2014 Optical Society of America

OCIS codes: (240.6680) Surface plasmons; (230.7408) Wavelength filtering devices; (230.7370) Waveguides; (130.3120) Integrated optics devices; (310.4165) Multilayer design.

http://dx.doi.org/10.1364/OL.39.003227

Surface plasmon polaritons (SPPs) propagating along the metal–dielectric interfaces has been considered one of the most promising ways to guide and manipulate the optical signals in ultradense nanophotonic integrated circuits (PICs) [1]. In particular, the metal–insulator–metal (MIM) waveguides allow the highly confined surface plasmon modes to propagate in a sharp bend with low additional loss [2,3] and are able to be easily manufactured using existing nanofabrication techniques [4,5]. Among many MIM-based plasmonic components, a nanoplasmonic ring resonator is a key element to implement plasmonic filters for the applications of optical communications, signal processing, and preamplified optical receivers [6–9]. Most of plasmonic filters based on ring resonator structures have a Lorentzian-shaped transmission response, which is inappropriate for the all-optical network system and wavelength division multiplexing (WDM) application. The filter based on periodic ring resonators directly connected with the MIM waveguides has been numerically demonstrated to possess flat-top transmission bands [9]. However, passband ripples are obtained owing to the periodical structure, and a lack of a comprehensive approach to decide the design parameters also gives rise to additional computation time.

Here we propose a new MIM-based bandpass filter with cascaded rectangular ring resonator structure and systematically determine the appropriate design parameters based on the principles of thin-film bandpass filter designs. We use an Ag–air–Ag waveguide to demonstrate our design concept. The dielectric constant of silver is described by the five-term Drude–Lorentz model [10]:

$$\varepsilon(\omega) = \varepsilon_\infty - \frac{\omega_p^2}{\omega^2 + i\gamma\omega} - \sum_{n=1}^{5} \frac{\Delta\varepsilon_n \omega_n^2}{\omega^2 - \omega_n^2 + i\gamma_n\omega}, \quad (1)$$

where $\varepsilon_\infty = 1.0$ is the relative permittivity in the infinity frequency, $\omega_p = 2002.6$ THz is the bulk plasma frequency, and $\gamma = 11.61$ THz is a damping constant. ω_n, γ_n, and $\Delta\varepsilon_n$ are the oscillator resonant frequencies, the damping factors, and weighting factors associated with the Lorentzian peaks, respectively.

Figure 1(a) schematically depicts the fundamental rectangular ring resonator with its length of L and its width of W directly connected to the input and output waveguides. The output waveguide is symmetrically located on the opposite side of the resonator with respect to the input waveguide. The widths of the ring and the input and output waveguides are w_1, w_i, and w_o, respectively. Due to the symmetric structure, the corresponding equivalent T-lumped circuit by the transmission line model is simply shown in Fig. 1(b). The lumped parameters of Z_a and Z_b are defined as [11,12]

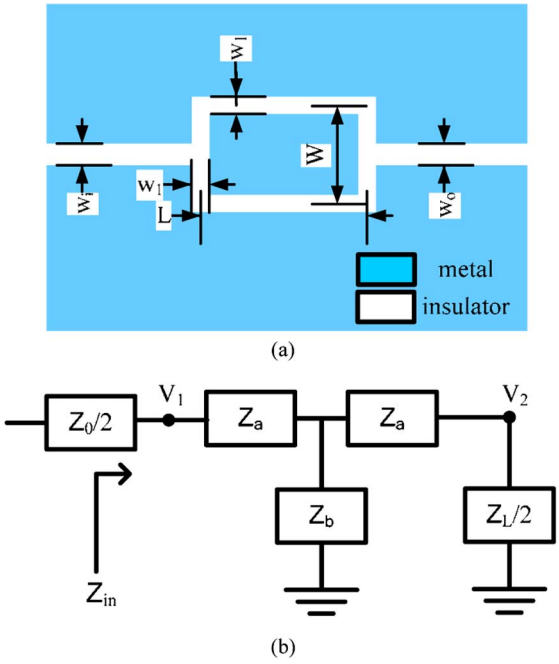

Fig. 1. (a) Schematic diagram of the directly connected rectangular ring resonator. (b) Corresponding equivalent lumped circuit.

$$Z_a = jZ_1 \tan(\beta_1 L_1/2) \tag{2}$$

and

$$Z_b = -jZ_1 \csc(\beta_1 L_1), \tag{3}$$

where β_1 is the propagation constant of the ring, L_1 is $(W + L)$, and Z_1 is the characteristic impedance of the ring, calculated by $Z_1 = (V/I) \approx (\beta_1 w_1)/(\omega \varepsilon_{\text{in}})$ with the permittivity of the insulator ε_{in} and the frequency of the incidence ω [13,14].

The transmission and reflection coefficients of this circuit, T and R, can be calculated as follows:

$$T = \frac{V_2^+}{V_1^+} = \frac{(1 + r_2)(1 - r_1)e^{-j\beta_1 L_1}}{1 - r_1 r_2 e^{-2j\beta_1 L_1}}, \tag{4}$$

$$R = \frac{V_1^-}{V_1^+} = \frac{r_1 - r_2 e^{-2j\beta_1 L_1}}{1 - r_1 r_2 e^{-2j\beta_1 L_1}}, \tag{5}$$

where V_2^+ and V_1^+ are the forward propagation voltages on the transmission lines of the output and input ports, respectively, and V_1^- is the backward propagation voltage on the input port: $r_1 = (2Z_1 - Z_0)/(2Z_1 + Z_0)$ and $r_2 = (2Z_1 - Z_L)/(2Z_1 + Z_L)$ with Z_0 and Z_L of the characteristic impedances of the input and output waveguides, respectively.

We see that r_1 and r_2 are the reflection coefficients of the corresponding T-shaped splitters, respectively [3]. Furthermore, Eqs. (4) and (5) are identical to the transmission and reflection formulations of a Fabry–Perot resonator, except that r_1, r_2, and β_1 are lossy. Therefore we can equal this ring structure to a one-cavity resonator with the reflection coefficients of mirrors r_1 and r_2 and the length of the cavity L_1.

It is known that a multicavity structure is conventionally used to accomplish a high-order bandpass filter. Accordingly, we cascade serial ring resonators to construct a multicavity structure, as shown in Fig. 2. Using the split-filter analysis, this structure becomes a generalized Fabry–Perot resonator by dividing it into two subsystem mirrors, A and B, separated by a cavity with a length of d [15]. Mirrors A and B can be described by their transmission coefficients t_A and t_B, and their reflection coefficients r_A and r_B with the reflectance phases ϕ_A and ϕ_B, respectively. Because two T-branch structures are included inside the cavity, the phase shift in the cavity becomes $\varphi = \beta_c d + \beta_A w_A/2 + \beta_B w_B/2$, where β_A, β_B, and β_c are the propagation constant of the w_A-wide ring in the mirror A next to the cavity, that of the w_B-wide ring in the mirror B next to the cavity, and that of the cavity C,

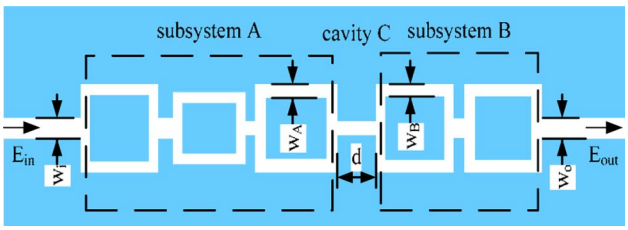

Fig. 2. Schematic illustration of a generalized cascaded rectangular ring resonator structure.

respectively. Then the transmission coefficient through the whole system is [16]

$$t_{\text{total}} = \frac{E_{\text{out}}}{E_{\text{in}}} = \frac{t_A t_B e^{-j\varphi}}{1 - r_A r_B e^{-j2\varphi}}, \tag{6}$$

where E_{in} and E_{out} are the complex amplitudes of the forward fields in the input and output waveguides, respectively.

The flat-top transmission band can be obtained as the total phase shift Φ along this structure has the following properties [16–18]:

$$\Phi = 2\,\text{Re}\{\varphi\} - \phi_A - \phi_B = 2m\pi, \tag{7}$$

$$\frac{d\Phi(\lambda_0)}{d\lambda} \approx 0, \tag{8}$$

where m is an integer, and λ_0 is the center wavelength.

To comply with the condition of Eq. (8), an anomalous dispersion (AD) mirror has to be used to generate a flat-top transmission band. An AD mirror with a one-cavity structure can be realized, as the reflectance of the input mirror is larger than that of the output one [16]. Its anomalous dispersion region in the reflection phase is obtained at the wavelength where the local minimal reflectance is located, called the resonant wavelength, i.e., the total phase shift inside the cavity $= 2m\pi$, $m =$ an integer. From Eqs. (4) and (5), both r_1 and r_2 are controlled by the width ratio of the ring to the input/output waveguide. As a result, to implement a one-cavity AD mirror, i.e., $|r_1| > |r_2|$, $w_i > w_o$ as w_1 is narrower than both w_i and w_o. Alternatively, $w_i < w_o$ as w_1 is wider than both w_i and w_o.

As an example of a plasmonic AD mirror, we designate $w_1 = 120$ nm, $w_i = 20$ nm, and $w_o = 100$ nm. Then L_1 is chosen such that $2\,\text{Re}\{\beta_1\}L_1 - \phi_{r1} - \phi_{r2} = 2m\pi$ at λ_0, where ϕ_{r1} and ϕ_{r2} are the phases of r_1 and r_2, respectively, and $m =$ an integer. In this case, L_1 is 725.8 nm for $\lambda_0 = 1550$ nm, roughly equal to the half-wave optical thickness because ϕ_{r1} and ϕ_{r2} are approximately either 0 or π radians. Let W and L be 350 and 375.8 nm, respectively, and its corresponding schematic diagram is illustrated in the inset of Fig. 3. Figure 3 shows the reflectance spectra and the corresponding reflection phase of this AD mirror. The reflectance spectra are both simulated by using a 2D finite-difference time-domain (FDTD) method and calculated by using Eq. (5). A commercial FDTD simulator (*Fullwave*, RSOFT Design Inc.) is used to calculate the performance of this device. The incidence is the fundamental TM mode of the MIM waveguide with its width of w_i. The grid sizes in the transverse direction, x, and transmission direction, z, are $\Delta x = \Delta z = 2$ nm, and the time step size is 4.67×10^{-18} s. We observe that a local minimum in the reflectance spectrum occurred at λ_0. Additionally, FDTD simulated results are roughly consistent with calculated ones by using Eq. (5), although the whole reflectance spectrum shifts to the wavelength of 1560 nm with relatively large values. On the other hand, an anomalous dispersion region ranging from 1370 to 1780 nm is observed, and the flat-top passband is expectedly obtained in this region [16,17].

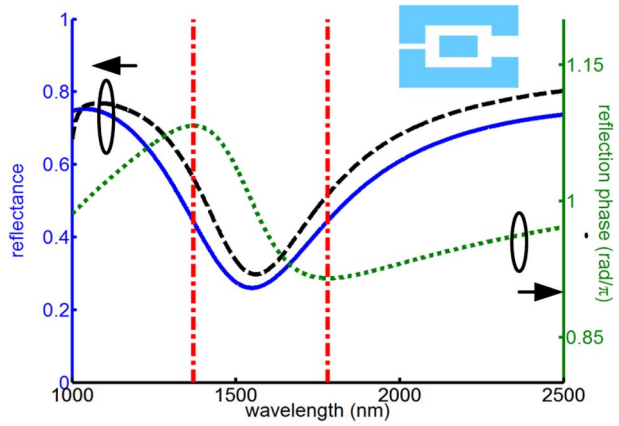

Fig. 3. Reflectance spectra obtained by using FDTD method (black dashed curve) and using Eq. (5) (blue solid curve) and the reflectance phase by using Eq. (5) (green dotted curve) of the AD mirror with $w_1 = 120$ nm, $w_i = 20$ nm, $w_o = 100$ nm, and $L_1 = 725.8$ nm. The inset is the schematic structure of the one-cavity plasmonic AD mirror.

Subsequently, we put these two identical AD mirrors opposite one another to accomplish a flat-top bandpass filter, as schematically drawn in the inset of Fig. 4(a). The cavity length d is 362.1 nm to satisfy the conditions of Eqs. (7) and (8). Figure 4(a) shows the transmission spectra of this structure both simulated by FDTD method and calculated by using Eq. (6). We observe an asymmetric transmission spectrum with slightly flat-top passband roughly centered at 1600 nm. This wavelength shift mainly is a consequence of the wavelength-dependent loss of the AD mirrors and dispersion of the surface plasmon modes. The maximum transmission is −1.12 dB at the wavelength of 1590 nm. The loss of this device mainly results from the transmission loss propagation through the ring resonators and the cavity. The FHWH is 545.7 nm, and the bandwidth at −0.5 dB transmission-deduction level is 350 nm. The simulated results closely agree with the calculated ones, except for a slightly narrow bandwidth with the FHWH of 453.3 nm and a smaller highest-transmission of −1.23 dB. This is because the dip width of the reflection spectrum of the AD mirror obtained by FDTD method is narrower than that calculated by using Eq. (5). Figure 4(b) shows the total phase shift Φ as a function of the wavelength, and we observe an approximately constant (∼0) at the wavelength of 1500–1600 nm, which is much narrower than the obtained flat

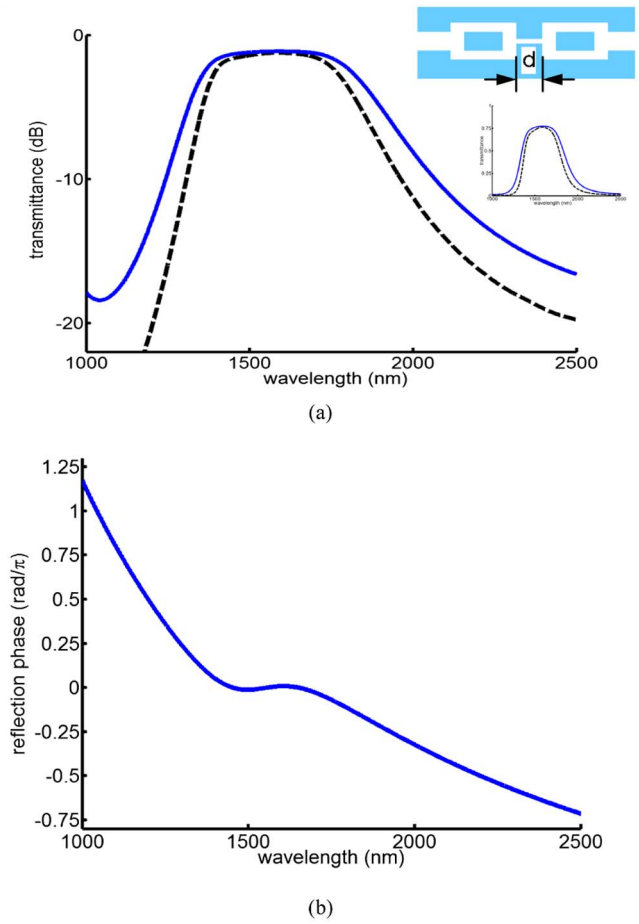

Fig. 4. (a) Transmission spectra of the bandpass filter with the cavity's length d of 362.1 nm simulated by FDTD method (dark dashed curve) and calculated by Eq. (6) (blue solid curve). Upper inset is the schematic of the simulated cascaded ring resonator structure. Lower inset is the transmission spectra in linear scale. (b) Calculated total phase shift inside the cavity C.

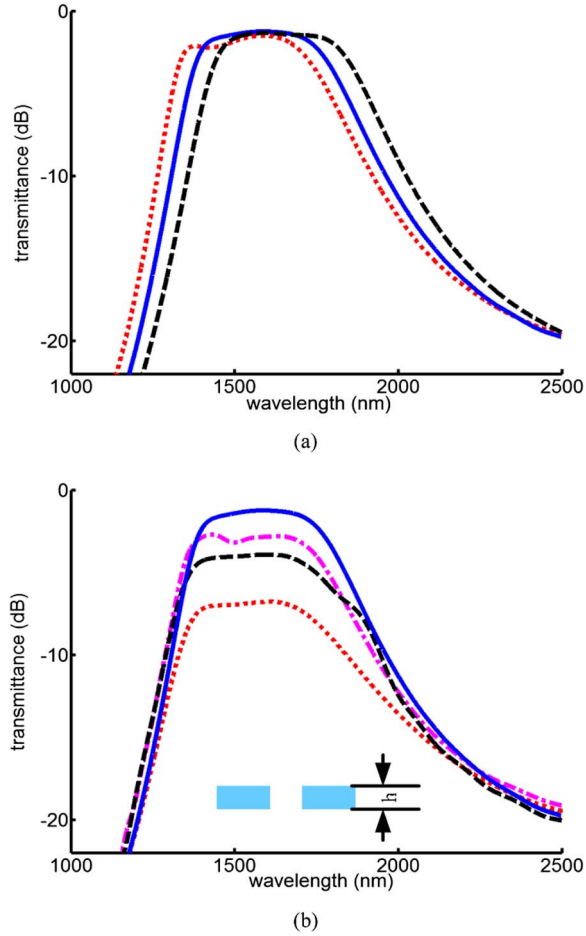

Fig. 5. Transmission spectrum variations with (a) different deviation ratios ζ:$\zeta = 0.95$ (red dotted curve), $\zeta = 1.00$ (blue solid curve), and $\zeta = 1.05$ (black dashed curve) and (b) different thicknesses of the metal film h: $h = 400$ nm (red dotted curve), $h = 1000$ nm (black dashed curve), $h = 1500$ nm (magenta dot-dashed curve), and 2D results (blue solid curve). Inset is the schematic of the 3D MIM waveguide structure.

region of the passband. This discrepancy is due to a shift in the center wavelength toward longer wavelength.

Supposed that all the geometrical parameters (i.e., W, L, w_1, w_i, and w_o) are varied by a deviation ratio ζ, and the transmission spectra of this filter simulated by FDTD method with $\zeta = 0.95$, 1 and 1.05 are illustrated in Fig. 5(a). As can been seen in Fig. 5(a), the transmission spectrum shifts to a longer wavelength as ζ increases, i.e., both W and L become larger. Besides, the shape of the passband is slightly distorted as a result of the mismatch of the condition in Eq. (8). The effect of finite-thickness MIM waveguides on the transmission spectrum of the aforementioned plasmonic filter is shown in Fig. 5(b), which is simulated by the 3D FDTD method. The cross-section of the MIM waveguide is shown in the inset of Fig. 5(b). The flat transmission band with degraded maximal transmittance is observed because of field scattering on the edges. With the increase of the thickness, the transmission spectrum tends to that of the 2D plasmonic filter, showing that our analysis and design approach can be applied for a realistic MIM plasmonic filter with thick thickness.

In summary, we have presented a flat-top bandpass plasmonic filter by cascading a sequence of rectangular ring resonators. First, using an equivalent circuit model, we find the performance of a directly connected rectangular ring resonator is similar to that of a one-cavity resonator. Additionally, the reflection coefficients of the mirrors in the resonator are controlled by the width ratios of the ring to the input and output waveguides. Then, by applying thin-film bandpass filter design methodology, a cascaded ring resonator structure is constructed to realize a bandpass filter with the characteristics of a squared passband. An example of the plasmonic AD mirror is designed by using a single ring resonator with $w_i < w_o$ and L_1 roughly of the half-wave optical thickness. Two identical aforementioned plasmonic AD mirrors are designed to obtain a flat-top bandpass filter, and the calculated results show that this filter possesses the maximum transmission of −1.12 dB, FHWH of 545.7 nm, and the bandwidth at −0.5 dB transmission-deduction level of 350 nm. The FDTD simulated results are closely consistent with the calculated ones. This design approach can be extended to carry out higher-order bandpass filters by using multicavity plasmonic AD mirrors comprised of cascaded ring resonators, and this plasmonic bandpass filter has great potential applications in nanoscale PICs.

References

1. E. Ozbay, Science **311**, 189 (2006).
2. T. W. Lee and S. Gray, Opt. Express **13**, 9652 (2005).
3. G. Veronis and S. Fan, Appl. Phys. Lett. **87**, 131102 (2005).
4. R. J. Walters, R. V. A. van Loon, I. Brunets, J. Schmitz, and A. Polman, Nat. Mater. **9**, 21 (2010).
5. P. Neutens, P. Van Dorpe, I. De Vlaminck, L. Lagae, and G. Borghs, Nat. Photonics **3**, 283 (2009).
6. A. Hosseini and Y. Massoud, Appl. Phys. Lett. **90**, 181102 (2007).
7. A. Setayesh, S. R. Mirnaziry, and M. S. Abrishamian, J. Opt. **13**, 035004 (2011).
8. T. B. Wang, X. W. Wen, C. P. Yin, and H. Z. Wang, Opt. Express **17**, 24096 (2009).
9. J. X. Tan, Y. B. Xie, J. W. Dong, and H. Z. Wang, Plasmonics **7**, 435 (2012).
10. A. D. Rakic, A. B. Djurisic, J. M. Elazar, and M. L. Majewski, Appl. Opt. **37**, 5271 (1998).
11. K. Chang and L. H. Hsieh, *Microwave Ring Circuits and Related Structures* (Wiley, 2004).
12. C. H. Chen and K. S. Liao, Opt. Express **21**, 4036 (2013).
13. S. E. Kocabas, G. Veronis, D. A. B. Miller, and S. Fan, IEEE J. Sel. Top. Quantum Electron. **14**, 1462 (2008).
14. H. Nejati and A. Beirami, Opt. Lett. **37**, 1050 (2012).
15. A. Thelen, *Design of Optical Interference Coatings* (McGraw-Hill, 1989).
16. C.-H. Chen, K. Tetz, W. Nakagawa, and Y. Fainman, Appl. Opt. **44**, 1503 (2005).
17. C.-H. Chen and Y. Fainman, IEEE J. Sel. Top. Quantum Electron. **13**, 262 (2007).
18. Y. V. Troitski, Appl. Opt. **34**, 4717 (1995).